Physics-Based Aggregate-Functions Approaches to Large Mom Problems

Ladislau Matekovits[1], Giuseppe Vecchi[1], Felipe Vico[2]
[1]Department of Electronics, Antennas and EMC Laboratory
(Laboratorio Antenne e Compatibilita Elettromagnetica - LACE),
Politecnico di Torino, Corso Duca degli Abruzzi 24, I-10129 Torino, Italy
ladislau.matekovits@polito.it , giuseppe.vecchi@polito.it

[2] iTEAM - Universidad Politcnica de Valencia, 46022 Valencia, SPAIN
fevibon@teleco.upv.es

***Abstract*—** Aggregate functions approaches construct efficient MoM basis functions by suitably grouping standard (e.g. Rao-Wilton-Glisson) functions. The application domains, objectives and related means of achieving them can be significantly different. In this paper we review some recent advances in aggregate-functions methods, putting them in a unifying perspective. We address matrix compression, multi-resolution sets, low- and high-frequency constructs. They can reduce the degrees of freedom of the problem so as to allow a direct, iteration-free solution, or can accelerate the convergence rate of iterative methods. We analyze compressive methods in more detail, providing general discussion and specific implementation examples.

***Index Terms*—** Integral equation techniques, Method of Moments, Large structures, Aggregate functions.

I. INTRODUCTION

The Integral Equation (IE) approach is widely used to solve antenna and scattering problems, and known for its effectiveness and robustness. The standard implementation of its Method of Moment (MoM) discretization has obvious limitations on the matrix size in terms of memory and CPU time for large scattering bodies and large and complex antennas and arrays. Less obvious, but very relevant are also issues related to the matrix conditioning, especially for very large problems or for problems with fine meshes, or mesh cells of very different sizes. In order to reduce the problem numerical complexity, two different families of approaches can be adopted: the first one consists in the so called fast methods that are based on the use of iterative solvers, and essentially act on the cost and memory occupation needed at each step of the iterative algorithm. Another class of methods is based on the grouping of basis functions into "aggregate functions" that are constructed in such a way to inject information about nature of the solution directly into the representation of the unknown currents.

Function aggregation, in turn, may take two different routes and perspectives. In one of its embodiment, aggregation may be used to reduce the number of degrees of freedom (DOF) of a problem; such a reduction may be so drastic as to make the direct solution of the MoM linear system is attainable even for very large and/or complex problems; when not possible, it will in any case make the use of iterative solvers more expedite. The other type of aggregate function approaches instead aim at improving the stability of the system, or to allow a sparsification of the resulting MoM matrix.

In this paper, we will address the aggregate function methods from a general perspective at first, showing that in all cases they add considerable flexibility to the MoM; this flexibility in turn allows to exploit the physical and mathematical properties of the underlying problem to the advantage of the computational complexity or stability of the solution. We will then focus our attention on methods that lead to a "compression" of the MoM matrix; two methods already proposed by these authors will be discussed in more detail for the sake of making clearer points. The two examined methods address different types of problems, and allow a broader perspective. The characteristics of the aforementioned algorithms

have been presented, or will be presented, in more detail in other works; the main scope of this paper is not indeed a detailed discussion of these particular methods but a more general review.

While this paper will be devoted to aggregate function methods, it is important to underline that fast methods and aggregate function methods are complementary. It is indeed possible to arrive at hybrid techniques that sum up the advantages of both approaches. A brief discussion on the prospects of these issues will be addressed where appropriate in the following sections.

II. THE AGGREGATE BASIS FUNCTION PARADIGM

Electromagnetic analysis of radiators or scatterers with arbitrary geometries requires the dicretization of the descriptive equations (EFIE, MPIE, CFIE, or GCFIE) by basis functions defined on subdomains.

The unknowns will in general comprise both electric and magnetic currents; for the sake of simplicity here we will however refer to the electric current only, denoted by $\underline{J}(\underline{r})$. The unknown is initially approximated by a set of basis functions defined on the meshed structure; most often these will be RWG on triangular patches, and/or piecewise-linear functions on wire segments; we will denote these standard basis functions $\left\{ \underline{f}_n(\underline{r}), n=1,...,N \right\}$ as "elemental" basis functions, and $\underline{J}^e$ is the approximation obtained with such a basis:

$$\underline{J}^e(\underline{r}) = \sum_{n=1}^{N} I_n \underline{f}_n(\underline{r}). \tag{1}$$

The key of function aggregation is to look for a different basis, of dimension M,

$$\underline{J}^a(\underline{r}) = \sum_{k=1}^{M} i_k \underline{\psi}_k(\underline{r}) \tag{2}$$

constructed with the elemental functions,

$$\underline{\psi}_k(\underline{r}) = \sum_{n=1}^{N_k} U_{nk} \underline{f}_n(\underline{r}). \tag{3}$$

The new basis functions $\left\{ \underline{\psi}_n(\underline{r}), n=1,...,M \right\}$ are called "aggregate" basis functions, and are combinations with fixed weights U_{nk} of the elemental basis functions $\underline{f}_n(\underline{r})$.

The new basis must of course present desirable numerical properties; this is discussed below. Also, one wants that the two bases yield the same accuracy, i.e. $\underline{j}^a = \underline{j}^e$ within the accuracy of both with respect to the actual solution.

Equation (3) describes the basis change from the initial elemental basis to the aggregate basis. We consider the initial MoM system for the elemental basis in (1)

$$\underline{J}^e(\underline{r}) = \sum_{n=1}^{N} I_n \underline{f}_n(\underline{r}) \quad \rightarrow [Z][I] = [B], \tag{4}$$

and the MoM for the aggregate basis (3)

$$\underline{J}^a(\underline{r}) = \sum_{k=1}^{M} i_k \underline{\psi}_k(\underline{r}) \quad \rightarrow [z][i] = [b]. \tag{5}$$

The basis change can likewise be written in terms of matrix operations via (3),

$$\underline{\psi}_k(\underline{r}) = \sum_{n=1}^{N_k} U_{nk} \underline{f}_n(\underline{r}) \quad \rightarrow [X] = \left[[U_1], ..., [U_M] \right]. \tag{6}$$

With this notation, application of the Galerkin testing with ψ_k to the initial Integral Equation leads to the relationship between the MoM matrices for the two bases:

$$[I] = [X][i], \quad [z] = [X]^H [Z][X], \quad [b] = [X]^H [B], \tag{7}$$

that clearly defines a basis change operation. In the above, we have considered the general case of complex-valued coefficients in the aggregation; the hermitean (^{H}) adjoint (conjugate transpose) reduces to transpose operation (^{T}) for real coefficients.

The general description of the method presented above includes all kinds of aggregation (and specifies none). As a general remark, note that all aggregate function schemes allow the re-use of MoM codes, and they are kernel-independent; this is a strong advantage of this class of approaches.

On the basis of the values of *N* and *M*, we differentiate between two fundamental cases as follows.

II.1 M = N: One-to-one basis change

In this case the dimension of the system remains unchanged, but the matrix in the aggregate function basis exhibits "better" properties: sparse matrix, faster convergence, etc.. To be practical, the (square) basis-change matrix [*X*] must obviously be very sparse.

The two bases $\{\underline{f}_n(\underline{r}), n = 1, \ldots, N\}$ and $\{\underline{\psi}_n(\underline{r}), n = 1, \ldots, N\}$ now span the same space, and with infinite-precision arithmetic the two solutions should be identical, $\underline{j}^a = \underline{j}^e$. However, when the aggregate basis is used to solve problems of the standard elemental basis, it might not be so, and $\underline{j}^a$ may be closer to the actual solution or more stable.

A classical example is the Helmholtz (Hodge) decomposition employed to avoid the low-frequency ill-conditioning of RWG (and wire) bases. This leads to the loop-star or loop-tree decompositions (e.g. [1, and references therein]); the MoM matrix in the aggregate basis has a far better conditioning.

Another important instance of this class of aggregate functions is the Multi-Resolution approach, where wavelet-like properties are introduced into the set of basis functions. Earlier applications of wavelet constructs were limited to simple geometries and mostly 2D scattering problems; in those cases wavelet functions similar to those employed in signal processing were used. More recently, realistic geometries have been addressed, either in planar or 3D cases; this has forced the wavelet functions to be significantly simpler, and the most successful approaches have managed to construct multiresolution functions as linear combinations of standard elemental basis functions: this ensures applicability to all those cases that can be analyzed by the employed elemental basis functions (e.g. RWG).

The first attempts addressed planar structures that can be discretized by rectangular cells [8] [9], [10], [11]; more recent approaches have addressed triangular cells [13], [12], [14], [15], [16].

In the early days, the motivation for MR approaches was the hope to ”sparsify” the MoM matrix, i.e. of achieving a high dynamic range of matrix entries that allows clipping smaller elements within a given accuracy bound. More recent works [10], [12], [16] have focused on the spectral properties of the resulting MR-MoM matrix, and the intrinsic pre-conditioning potential of the MR basis; the reasons of this pre conditioning effects are addressed in [17]. In all the above examples, aggregate functions are real.

II.2 M << N: compression

In this case the dimension of the system described by the aggregate functions is reduced, which corresponds to having the reduced degrees of freedom (DOF) of the solution. As will be discussed later on in Sec. III., this does not imply per se the necessity to reduce the accuracy. It is however important to assess the overhead introduced by the compression scheme into the overall solution, for a given degree of accuracy. For a given accuracy, the degree of compression and the overall efficiency depend on how the aggregate functions are generated; it is intuitive that it is important to incorporate information on the physical nature of the problem under analysis to affect this choice efficiently.

Since in this case the dimension of the system can be drastically reduced, even of orders of magnitude, the primary computational gain is achieved during the factorization of the system matrix in the reduced basis. Low memory occupation, the possibility to employ a direct solver, and with the ability to treat multiple right hand side (RHS) at marginal costs are the immediate advantages. The reduced number of DOF also preludes to a faster convergence of iterative solvers, if a direct solution is not viable. While memory occupation can be significantly reduced, the matrix fill time is not addressed directly. The aggregate nature of the basis functions, however, lends itself to various schemes to exploit fast matrix-vector multiplications to this aim, as discussed later on.

The overhead comes from two parts of the procedure: a) generation of the aggregate function basis; b) basis change in (7). Using standard matrix-vector products, it is $O(MN(M + N)) \approx O(MN^2)$, i.e. much less than the N^3 of the LU factorization. With fast matrix-vector products, this is reduced accordingly.

Works that belongs to this class where first developed for planar structures, and then extended to 3D problems [2], [3], [4], [5], [6], [7]; a com prehensive survey can be found in [7]. Aggregate functions have been termed with different names along the ”history” of this approach: diakoptic [2], ”macro” basis functions (MBF) [4], synthetic basis functions [6], [7], and characteristic basis functions (CBF) [5]. All of these methods are in essence domain-decomposition methods, i.e. they are based on the solution of the initial problem on

parts of the overall structure, and employ this information in constructing the aggregate functions; the aggregate functions, in turn, are defined on sub-domains larger that the individual mesh cells and smaller than the entire structure. The more recent Wave-front Basis Function (WBF) method [24, and references therein] is slightly different. It addresses very large scattering problems, and employs phase information on the asymptotic (high-frequency) solution to construct the aggregate functions. While the associated aggregate functions are still defined on subdomains, the associated geometric partitioning has different (much less stringent) needs as in the case of the previous groups of methods. In what follows, we will discuss compression-type aggregate function schemes only.

III. COMPRESSION SCHEMES

III.1 General features

We begin by observing that the use of compressive aggregate-function bases is equivalent to the use of the space spanned by the elemental basis functions to approximate the unknown, but leaving only certain subspaces accessible to the solution algorithm. This can be seen from equations (4-7), and noting that the basis-change matrix [X] is $N \times N$. The specificity of the aggregate function algorithms is indeed in choosing and constructing these subspaces in which the solution is sought.

In particular, we assume that the initial discretization is accurate enough and can be considered "exact" (i.e. we do not count on the improvement on condition number and stability that the compression scheme might allow). If we denote the concerned spaces by

$$\begin{aligned} &\underline{J}^e \in H_N^f, \quad H_N^f = \text{span}\left\{\underline{f}_n, n=1,...,N\right\} \\ &\underline{J}^a \in H_M^\psi, \quad H_M^\psi = \text{span}\left\{\underline{\psi}_n, n=1,...,M<N\right\}, \end{aligned} \tag{8}$$

because of (3), $[X] : H_N^f \to H_M^\psi$; since $M < N$ it is apparent that $H_M^\psi \subset H_N^f$. Per se, this does not prevent the equality $\underline{j}^a = \underline{j}^e$, but that depends on whether the "exact" solution $\underline{j}^e$ lies in the subspace $H_M^\psi \subset H_N^f$.

It is the experience of the authors, that it is often counter-intuitive that a reduction of the DOF may be done without sacrificing solution accuracy. This issue is best addressed after two specific examples of compressive aggregate-functions methods are discussed, and will be addressed in Sec. III.4.

As mentioned previously, most methods of present interest can be considered domain-decomposition (DD) methods, i.e. methods in which the solution for the entire structure employs partial solutions for isolated parts of the entire structure to reduce the overall size of the problem. Domain-decomposition (DD) methods are well known and employed in finite-element solutions of differential problems (FEM) (a review of the related literature is outside the scopes of this work). There, DD is directly feasible (albeit far from trivial) thanks to the local nature of the interactions between basis functions that constitute the (exactly sparse) system matrix. In integral equation formulations no interaction is local, and this makes the DD effort more complex.

The first step of a DD method is the subdivision of the overall structure into portions, here called "blocks". Next, the electromagnetic (EM) problem is solved on these blocks, taken in isolation. Finally, these solutions are used to compute, at a reduced cost, the solution for the entire structure. Having to "patch up" the solutions on individual blocks, three issues are crucial for an effective method.

1. Specify the forcing terms when solving for the isolated blocks;
2. Ensure continuity of the solution across boundaries of neighboring, contacting blocks (when present);
3. Avoid the artifacts arising from the solution for isolated blocks when these originate from "tearing" an otherwise continuous surface. When treated as isolated, a block will have edges at which a correct solution of the EM problem exhibits a singular behavior; this latter constitutes an obvious artifact when patching up the structure, in which the inter-block boundary is not an edge.

The above steps and issues are common to all methods of the explicit DD type (SFX, CBF, MBF, diakoptics); the way these steps are performed, and how the above issues are tackled is precisely at the root of the differences for the various approaches.

In the following we present two instances of implementations of the compressive aggregate function scheme: the Synthetic Function eXpansion (SFX) approach and the Wavefront Basis Method (WBF).

As alluded in the Introduction, the details of the methods being presented do not belong to this paper; their main steps will be however be reported here for the sake of clarity, with the objective of putting them in perspective.

It can be observed that compressive aggregate function methods reduce memory storage requirements to the size of the largest block in the DD, and will drastically reduce solution times. However, function aggregation does not reduce per se the MoM filling time. However, as mentioned in the Introduction, aggregate function methods are conveniently coupled to fast methods to this end. While not claiming any literature completeness, one can report that macro-basis functions have been coupled to the Fast-Multiple Method (FMM) [18]; SFX has been coupled to AIM [19] and a multi-grid strategy [20]; CBF has been coupled to FMM [21] and to the Adaptive Cross Approximation (ACA) [22].

On the other hand, the Wavefront Basis Method (WBF) is naturally posed to be used in conjunction with a fast method.

III.2 The Synthetic Function Expansion (SFX) Approach

We now describe how the above general DD predicaments are implemented in practice, using the SFX method as example. The method is described in [6], and in [7] in a detailed manner: here we will only briefly summarize the key aspects. For the sake of readability, we will refrain from referring to the above-cited papers in describing the method here.

In the SFX approach, the DD step is followed by the identification of surface blocks (s-blocks) and line-blocks (l-blocks). The s-blocks are formed by all mesh cells (triangles) that geometrically constitute a block; the l-blocks are the mesh edges (segments) that are in common between two adjacent blocks; they are absent when the block subdivision does not generates ”cuts” in the metal (e.g. for isolated radiators in an array). This is the first step taken to address the current continuity across blocks. An example of this division is shown in Figs. 1 and 2.

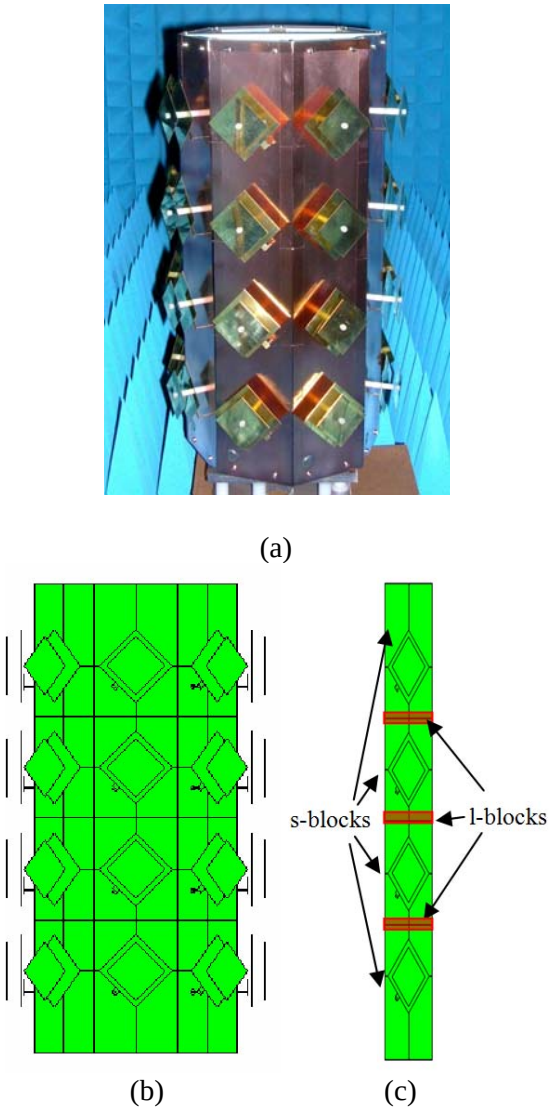

Fig. 1. Conformal base station antenna. (a) Photograph, (b) CAD model, (c) CAD model of the single column, with example indications of s-blocks and l-blocks.

It is important to stress that while unknowns are surface currents, the blocks have to be thought in terms of volumes that include the surfaces where the unknown currents reside; this allows to employ the (surface) Equivalence Theorem on the bounding box of the block. With this setting, the DD problem can be set in terms of coupled equations that involve the sources on the bounding box; in SFX, these are not treated as unknowns, but employed as forcing terms for the EM problem of the block in isolation (see Fig. 2 for an example).

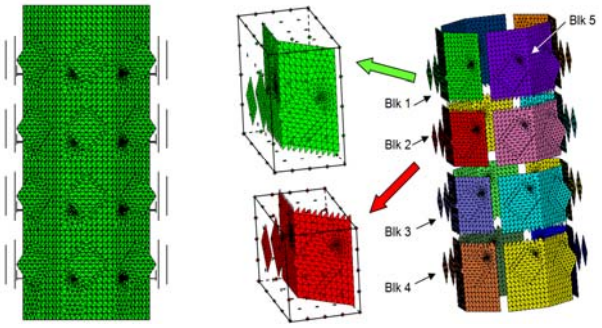

Fig. 2. CAD model of the conformal base station antenna: (a) Meshed geometry, (b) block separation used when analyzing it with SFX technique with the auxiliary sources around the Blocks 1 and 2 respectively.

Thanks to the Equivalent Theorem setting, if enough sources are considered, a linear combination of all the responses to the forcing terms on the bounding box will be able to correctly represent any currents inside the block, including the exact solution of the complete problem. Hence, if these responses are used to construct the aggregate basis functions the subspace $H_M^{\psi} \subset H_N^f$ will contain the desired solution. In order to make the procedure robust and efficient, an SVD is employed to retain those terms that are linearly independent (to a specified degree). The aggregate functions defined on the blocks of the structure are called "Synthetic Functions" (SF).

With respect to the notation set in the previous section, the SF generation procedure can be summarized as follows. The conductor surface S is divided into N_{SB} portions S_s, s = 1, ..., N_{SB} ($S = U_{s=1}^{N_{SB}} S_s$), the above-mentioned s-blocks (surface blocks); on each block, there will be $K_s << N$ unknowns. Some s-blocks may be contacting, i.e. a portion of their boundary may be shared with another s-block; these N_{LB} line segments are the l-blocks (line blocks).

The SF are defined on the s-blocks; this leaves out the individual elemental functions defined on the edges belonging to l-blocks. So far, these functions are left unconstrained as unknowns (i.e. not organized in aggregations). This allows a considerable flexibility in enforcing current continuity across blocks, which is naturally achieved – provided the above alluded spurious edge effects are not present.

In order to avoid artifacts due to edge-singularities in the single-block solution, the (edge) boundary condition has been modified on l-blocks; on these segments, half-RWG functions are inserted during the solution for the single-block problem, and deleted henceforth. This approach locally approximates a short-circuit (electric wall) condition, that effectively deletes the edge-singularity, and preludes to a successful current continuity. On the s^{th} s-block we will indicate by L_s the total number of these half-RWG. When solving for a block in isolation, there will therefore be $K_{Ts} = K_s + L_s$ unknowns.

In order to compute the responses that will lead to the SF, sources have first of all to be placed at the block feeding ports (if any is present); they will be called "natural", and their number (for the s^{th} block) denoted by N_{nat}^s; in case the problem entails an incident-wave forcing term, this will substitute for the port feeding as a natural source. Coupling with the rest of the structure is accomplished by considering two other types of sources.

- Sources placed on the block boundary, that are called "coupling" sources; their number (for the s^{th} block) is denoted by N_{coup}^s. They are conveniently implemented as RWG, which allows re-use of the modules of any MoM code to compute the RHS of the single-block problem.

- If l-blocks are present (i.e. the block periphery cuts a solid metal of finite extent), sources have to be placed along that periphery, called "connection" sources. They can be simply half-RWG, which simplifies the implementation. According to the previous discussion, on the s^{th} block there will N_{con}^s such sources.

The total number of sources on each block is therefore $N_S^s = N_{nat}^s + N_{con}^s + N_{coup}^s$. Each of these sources will constitute a RHS [$B_s^{(k)}$], k = 1, ..., N_S^s for the problem (1, 4), but limited to the number $K_{Ts} = K_s + L_s$ of the unknowns on the block. Denoting by $[Z_{B,s}]$ the pertinent MoM matrix of

the problem, [$r_s^{(k)}$] the response to k^{th} source and omitting the block index for simplicity, the responses are defined by

$$[Z_B][r^{(k)}] = [B^{(k)}]$$

The responses are next assembled into a matrix

$$\left[R\right] = \left[\left[r^{(1)}\right], ..., \left[r^{(N_s)}\right]\right]$$

and an SVD is performed on it, resulting in

$$[R] = [U][\rho][V]^{\text{H}} \qquad (9)$$

Each column of $[U]$ identifies the coefficients of one aggregate function in (6); the most relevant (largest) $N_{s,SF}$ terms are kept (note re-introduction of the block index s), and constitute the basis for the SF eXpansion (SFX) of the solution. In [7] an extensive study of the threshold used for the determination of the number of SFs has been presented. It is necessary at this stage to introduce the notion of SF (singular vectors) "associated" to a given type of source. While the SVD orthogonalization does not allow to identify an exact, direct correspondence between the sources and the SF, this relationship often exists approximately. In quantitative terms, a SF described by column $[U_j]$ is related to source k when the projection $[U_k]^H[r^{(j)}]$ is significantly larger than for all other responses. The correspondence is still stronger when one collectively considers homogeneous groups of sources and SF, e.g. natural, coupling, and connections. This justifies the ensuing terminology of "natural SF", "coupling SF", and "connection SF".

The scheme always calls for the inclusion of all N_{nat} natural SF; the number of the remaining SF to be kept is conveniently related to a thresholding of the SV sequence ρ_1, ρ_2, ..., ρ_{NS} . Upon fixing a threshold t, we will keep all SF associated to SV that satisfy

$$\rho_n / \rho_{N_{nat}} \le t \,. \qquad (10)$$

Examples of convergence studies and thresholding are given in Sec. IV.; convergence with respect to the employed number of coupling sources was studied in [7].

As to the SV thresholding issue, some general comments can be made:

- The threshold is problem dependent; very often the SV sequence has visible features that can guide a "manual" or automatic selection, like a clear jump or a clear change of slope. For example, if the block bounding box is the far region of [23], there is a jump in correspondence with the number of degrees of freedom of the radiated field; the latter is seldom observed in most practical problems, especially when the DD effects a "tearing" of the metal structure; nonetheless, the above example shows that the SV sequence depends on the physical structures, not on the source selection.

- The SV sequence and the effect of thresholding are expected to be different in antenna and scattering problems. Aside from the block-toblock interactions due to the cuts (discussed above), in antenna problems there will be often interaction between non-contacting but near features belonging to different blocks. The level of accuracy required in scattering problems is lower than required in antenna problems: these impacts on the threshold value selection. In this sense, it is very important that the convergence with respect to t be uniform, so that one can choose to be conservative in the absence of better knowledge. While no mathematical proof of uniform convergence can be presently offered for any of the existing compressive methods, the case studies in [7] and in Sec. IV.1 have always exhibited this convergence for SFX.

- When the DD calls for tearing of metal portions, it is to be expected that connection sources have almost the same importance as natural ones; therefore, to be on the safe side one can always include

$$Q = N_{nat} + N_{con}$$

SF_s, and start counting the SV threshold from that point; this corresponds to the modified threshold parameter

$$\rho_n / \rho_Q \le T \qquad (11)$$

- Finally, we remark that the ratio between total number of SV and actual number of kept term is not necessarily an indication of numerical efficiency. As a matter of fact, the ideal situation knows exactly how many sources are necessary, which makes the abovementioned ratio one. This should be kept in mind, e.g., when interpreting the thresholding study in

Sec. IV.1. On the opposite end, the maximum dynamic range in the SV of the kept terms depends on the "noise floor", i.e. machine precision and accuracy of the implemented SVD algorithm.

III.3 Wavefront Basis Method (WBF)

This technique is a new approach to solve very large scattering electromagnetic problems based on the MoM. The method can be seen as an extension of the Asymptotic Phase front Extraction (APE) approach to MoM [25] - [29]. In what follows we will report on the key points of the method, and present preliminary results for 2D scattering problems. The presentation of WBF here is functional to exemplifying how the aggregate function paradigm can conveniently comprehend approaches of very different nature, and to discuss the issue of the DOF and the related sub-space choice. A more comprehensive description of the method will be presented in a forthcoming paper.

The Asymptotic Phasefront Extraction (APE) method is based on the observation that most of the degrees of freedom in the MoM are used just to follow the fast variation of the phase of the solution, while its amplitude varies on a much slower scale,

$$\underline{J}\left(\underline{r}\right) = \underline{J}_{slow}\left(\underline{r}\right)\exp\left(jk\Phi\left(\underline{r}\right)\right), \qquad (12)$$

so that it can be correctly described by much fewer basis functions having a multi-wavelength support. The APE produces a huge reduction in the matrix size, but matrix filling time is drastically more expensive due to the highly oscillatory behavior introduced by the inserted phase terms; overcoming this difficulty is the subject of several papers that we refrain to review here. The extraction of the "asymptotic" phase function is a key issue. For smooth convex scatters the PO phase appears to be sufficient, while the issue for convex scatterers remains essentially open.

In the present approach [24], we employ the aggregation paradigm to construct the multiwavelength basis functions of APE starting from standard basis functions. In line with the aggregate functions approach discussed above, we consider our approach as an add-on to a fast MoM, of which it affects a compression. A key component of the method is the (novel) method for extracting the phase front of the induced currents, which leads to "Wavefront Basis Functions" (WBF) aggregate functions. It is essentially a kind of numerical Beam Tracing performed with algebraic operations on the standard MoM matrix. This process permits reusing standard Fast-MoM codes as FMM or AIM. The method will be presented with specific reference to 2D scattering problems (TE incidence), and results will be presented for this case; because of the scalar nature of the problem, with respect to the previous sections we will drop the vector sign in all relevant notation. It can be extended to 3D problems; due to the algebraic nature of the procedure, most of the extension steps are straightforward, and we will briefly discuss those issues that are not obvious.

The problem is initially discretized with standard (sub-wavelength) basis functions as in (1); in the 2D problem explicitly considered, these are piece-wise triangular (PWT) functions. It is convenient to indicate them as $f_n\left(\underline{r};l\right)$ where the second argument is their (sub-wavelength) length l; as for the other aggregate-function methods, these will be termed "elemental" basis functions. Next, one approximates the slow variation of the solution with the same type of functions used for the initial discretization (RWG or PWT), but of much larger, multi-wavelength extent; this is conveniently expressed as

$$J_{slow}\left(t\right) = \sum_{m=1}^{M} I_m^{slow} f_m\left(\underline{r};L_m\right), \qquad (13)$$

where $f_n\left(\underline{r};l\right)$ is the (phaseless) amplitude behavior of the (large) functions, that have the same expression of the elemental functions but different (multi-wavelength) support L. The definition of the aggregate functions follows from insertion of (12) and (13) into (1); the terms $f_m\left(\underline{r};L_m\right)\exp\left(jk\Phi\left(\underline{r}\right)\right)$ are conveniently approximated using the elemental basis functions, apt to represent the fast variations of the solution J; that is, one can write

$$f_m\left(\underline{r};L_m\right)\exp\left(jk\Phi\left(\underline{r}\right)\right) = \sum_{p=1}^{Km}\exp\left(jk\Phi\left(\underline{r}_p\right)\right) f_p\left(\underline{r};L_p\right)$$

where $\underline{r}_p$ is the center of the p^{th} elemental basis function; comparison with (2) and (6) yields

$$\psi_m(\underline{r}) = F_m^{AP}(\underline{r}) = \sum_{p=1}^{Km} U_{p,m} f_p(\underline{r}; L_p)$$
$$U_{p,m} = \exp\left(jk\Phi(\underline{r}_p)\right) f_m(\underline{r}; L_m) \quad . \qquad (14)$$

The aggregate functions $\psi_m(\underline{r}) = F_m^{AP}(\underline{r})$ have multi-wavelength support, and this results in a drastic compression of the standard MoM matrix. These functions are the "Wavefront Basis Functions" (WBF) to be discussed here; a pictorial description of the WBF can be found in Fig. 3. The geometric aggregation underlying theWBF is trivial in the 2D case; in 3D it requires geometric aggregations like those employed in the oct-tree partitioning employed for fast multi-level methods; two different examples of how to do it can be found in [15] and [16](the aggregation is carried out with a different aim in these works).

We observe that the aggregate (multiwavelength) functions are overlapped; this makes enforcement of current continuity on sub-domains a non-issue.

With reference to the setting in Sec. III.1, one can observe that the method above is equivalent to look for a solution in the subspace $H_M^{\psi} \subset H_N^f$ with the pre-calculated asymptotic phase. Therefore, the accuracy of the method hinges about this Ansatz, and the ability to correctly estimate this phase.

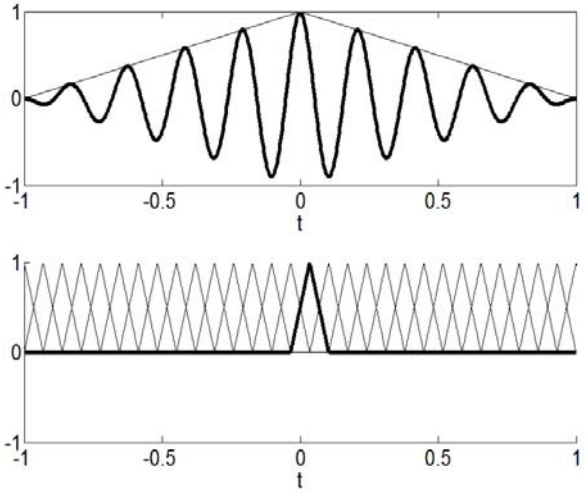

Fig. 3. WBF Aggregate basis function (top; real part) as linear combination of standard (sub-wavelength) basis functions (bottom).

Next, we use a Galerkin scheme with respect to the M aggregate functions. Assembling the basis change in algebraic form as in Sec. Sec. II., we have

$$[z] = [Z_{HF}] = [X_{HF}]^H \cdot [Z] \cdot [X_{HF}]$$
$$X_{HF} = \begin{bmatrix} U_{1,1} & & & \\ . & U_{1,2} & & \\ U_{k1,1} & . & & \\ & U_{k2,2} & . & U_{1,M} \\ & & . & . \\ & & & U_{kM,M} \end{bmatrix}, \qquad (15)$$

where $[X_{HF}]$ is sparse because two non-adjacent (aggregate) basis functions have disjoint support; each column has a number of non-zero terms independent of *N*. Note that one can use standard fast MoM codes to compute the vector-matrix products in (15). Very often the number M of aggregate basis functions is small enough to allow a direct solution for the compressed matrix Z_{HF} ; in all other cases, the above is used in the iterative solver. The compressive effect of the WBF produces a strong acceleration of the convergence.

Before proceeding further, we add that in most practical problems there will be sharp features (like the edge of a reflector) where the Ansatz (12) is questionable. This is solved in a simple manner by adding (unconstrained) elemental basis functions around these sharp features, which will add up to the count of the DOF like the unknowns associated to connection functions in SFX.

When the scatterer is flat or smooth and convex, PO is usually a good approximation for the phase; in this case, the above is directly applicable. The proposed algorithm, however, allows to go further. While a detailed description is beyond the scope of this work, the phase-tracking algorithm is outlined next in its salient traits.

One starts with the WBF with local PO phase. These will be zero-order WBF, ψ_k^0, described by coefficients $[U_k^{(0)}]$. Next, the radiation of all of these WBF_0 everywhere on the structure is considered; note that this is described by the product

$$[Z]\left[U_k^{(0)}\right]$$

that can be carried out by a fast matrix-vector multiplication. Because of the large support, the WBF radiate very narrow beams, and this is analogous to a beam shooting. The region(s) more intensely "lit" will constitute the support for the first-order WBF, as pictorially shown in Fig. 4; their phase will be that of the field radiated by the 0-th order WBF. The procedure is repeated with WBF or order 1 acting as "transmitter" to get the second-order WBF, and so on.

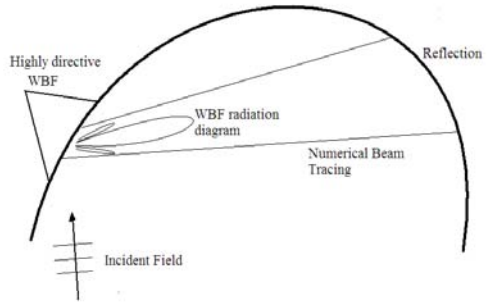

Fig. 4. Numerical Beam Tracing by iterating the operator of the EFIE.

2D tests of the method are reported in Sec. IV.2; in many instances it reduces the degrees of freedom to a very low value that is almost frequency independent, thus allowing a direct (iteration free) solution. Finally, we remark that a recent work [30] shares some of the objectives and approaches of this work.

III.4 Accuracy and DOF

It is often intuitive that a DOF reduction is possible when the solution is over-sampled. For example, in antenna problems one is often forced to employ mesh cells well below the $\lambda/5-\lambda/10$ rule employed in smooth scattering problems. It can thus be expected that a "smart" choice of the aggregate functions may tap into this redundancy to reduce the global DOF; for example, far interactions between aggregate functions will not need a fine detail to be accurately described. The above is correct, but it does not constitute the full picture.

A trivial, but somewhat revealing example is the following. If we take $M = 1$ and $\underline{\psi}_1$ to be the exact solution to the original problem, of course a 1-dimensional subspace is enough to allow the solution with compressive aggregate functions. No matter how trivial, this example points at the two key ingredients of a good compressive scheme: a) the aggregate basis functions must be related to the solution of the original boundary-value problem (hopefully, not in its entirety); b) the success of the method also depends on its ability in selecting the subspace of the aggregate-function solution in a way that depends on the properties of the forcing term (RHS).

In this perspective, one can observe that all compression schemes imply the use of aggregate basis functions that are "Maxwellian", in the sense that they are related to the (exact or asymptotic) solution of Maxwell's equations with part of the original boundary conditions.

The methods like SFX, CBS, etc., rely on the solution of the problem in parts of the original structures, and these solutions are related to the original forcing field. It can be noted that this obviously comes at a (computational) cost, and in general the higher this cost (e.g. the larger the sub-domains), the more accurate the solution. The issue is finding an optimal way of achieving accuracy at a low cost.

The WBF method relies on the asymptotic approximation of the solution; this solution is not used in its entirety, and only the phase is employed. As already commented, this phase information essentially bounds the supbspace determination, and is key in ensuring a correct solution. The dependence on the forcing term in the construction of the solution subspace is more evident in this technique than in the explicit DD schemes like SFX and CBF. However, in both SFX and CBF the forcing field plays a role in the construction of the aggregate functions; in these case, one often considers a certain number of incident plane waves as "natural sources"; in SFX and the case of an array, e.g., each block has its own natural source, which corresponds to considering all possible choices of port feeding.

Another vantage point can be gained by resorting to the SVD of the problems in (4) and (5):

$$\begin{aligned} [Z] &= \sum_{k=1}^{N} \zeta_k [u_k][v_k]^H \\ [I^e] &= \sum_{k=1}^{N} \frac{1}{\zeta_k} [u_k]\left([v_k]^H [B]\right) \end{aligned} \quad . \qquad (16)$$

As well known, the above indicates that the most relevant singular values (SV) of [Z] are the smallest, in the sense that for a *generic* RHS the smallest (SV) are those who determine the solution accuracy. Considering now the compressed matrix,

$$[z]=[X]^H[Z][X]=\sum_{k=1}^{N}\zeta_k[X]^H[u_k][v_k]^H[X]. \quad (17)$$

one understands that the aggregate functions must ideally all reside in the span of the singular vectors associated to the most relevant (i.e. smallest) SV. Note that this criterion is essentially independent of the forcing term, and is the option most typically followed in approaches like SFX and CBF, less oriented to tailoring the solution subspace around a specific forcing term.

IV. NUMERICAL EXAMPLES

In this section numerical results are presented to clarify the application of SFX and WBF. All the reported examples have been simulated on standard PC, equipped with a Pentium4 processor, with 2.3GHz clock and 512MB RAM.

IV.1 SFX

The SFX method was employed to design the conformal broad-band GSM-UMTS base station antenna shown in Fig. 1. It was designed for adaptive ("smart") operation. It is similar to, and inspired by the configuration in [31].

The structure has been chosen with the aim of applying the SFX method to a real-life geometry, and finally comparing simulation and measured results. The antenna requirements, design, and measurement procedure are outside the scopes of this paper; they are reported elsewhere, [32], [33] and in future communications; here we concentrate on the computational side and on the ensuing experimental validation.

The array antenna has 32 identical square stacked patches, in a 4 × 8 arrangement over an octagonal prism. Radiating elements are excited by proximity coupling with an L probe-strip structure, visible in the CAD model in Fig. 1. Excitation is modeled numerically via a voltage gap at the base of the probe, where it is connected to the (finite) ground. For SFX application, it is important to note that the underlying prism is a solid metal (the grounds of the facets are electrically connected).

In the full antennas, the 4 patches of each column are fed by a 1 : 4 equal-length, uniform-amplitude microstrip beam forming network printed below the ground plane; i.e., individual radiator are not accessible individually. One of the facets of the antenna in Fig. 1 (not shown there) was initially constructed with access to the four individual radiators; it will be used to compare simulation and measured results for S-parameters. The radiation results of the conformal array refer to operation with equal phase and amplitude over the eight columns (achieved via a commercial 1 : 8 uniform splitter).

At the center frequency, the antenna is about 3.1λ in height; the width of one facet is about 0.55λ while the average length of the edge of the stacked patches is of about 0.32λ. Its numerical model involves 24501 unknowns. We observe that no symmetry was used in the SFX simulation. A standard MoM solution in this case was unfeasible on the standard (32-bit) employed PC. The individual column, requiring 3010 unknowns, will thus be used for comparing SFX results to standard MoM.

Comparison between SFX and the standard MoM solution will be done with reference to the surface current relative error:

$$\varepsilon=\frac{\|I_{MoM}-I_{SFX}\|_2}{\|I_{MoM}\|_2}, \quad (18)$$

and directly on S-parameters or radiation pattern.

Analysis of the single column

The block partitioning of the facet is shown in Fig. 1c; it can be noted that there is one radiator per block, and that the block boundary cuts the (finite) ground, thus requiring the use of l-blocks and connection functions. It can be observed that the blocks are pairwise identical, the difference being on whether the block is central (bordering with one block per side) or on the edge. The coupling sources were placed on a regular grid on the (cubical) bounding box (not shown; an example of source distribution is shown for the full antenna below). The reported result refers to a total of 98 *coupling* sources on the block boundary for all blocks.

In counting SV and SF, it should be kept in mind that the present implementation employs real

(as opposed to complex) response vectors, i.e. separating their real and imaginary parts prior to the SVD operation in (9); the reasons for this (not critical) choice are detailed in [7]). This makes the association between SF and sources to appear typically in pairs.

The SV sequences for the four blocks are shown in Fig. 7, and the associated convergence of the solution vs. SV truncation threshold t (in (10)) is shown in Fig. 8. The convergence for the radiation pattern is in Fig. 5. Comparison of S-parameters results for standard MoM and SFX are shown next in Fig. 6 for $t \approx 10^{-3}$.

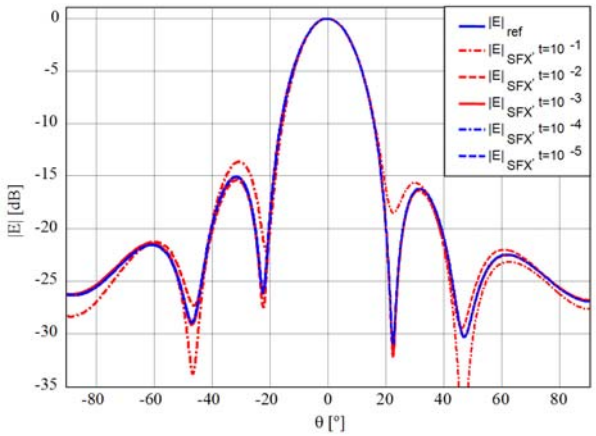

Fig. 5. Single column 4-patch array: radiation pattern convergence vs. SV truncation threshold t. The graph shows the cut along the array longitudinal axis. Solid blue line: reference; the other curves refer to the t value reported in the inset.

In order to interpret the results, we detail the relevant numbers for this case. We have one natural port on all blocks, i.e. $N_{nat}^{1,2} = 1$, while the number of connection functions is $N_{con}^{1} = 20$ and $N_{con}^{2} = 40$ on block 1 and 2 respectively. We have therefore $Q_1 = 42$ and $Q_2 = 82$ for the two types of blocks, having factored in the 2 factor for real/imaginary splitting; the position of these numbers in the SV sequences in Fig. 7 is indicated for further reference.

It is important to observe that the solution convergence is monotonic with respect to the number of considered SF; this is a guarantee of stable solution. The convergence analysis shows that keeping as many SF as natural plus all connection sources is a conservative estimate.

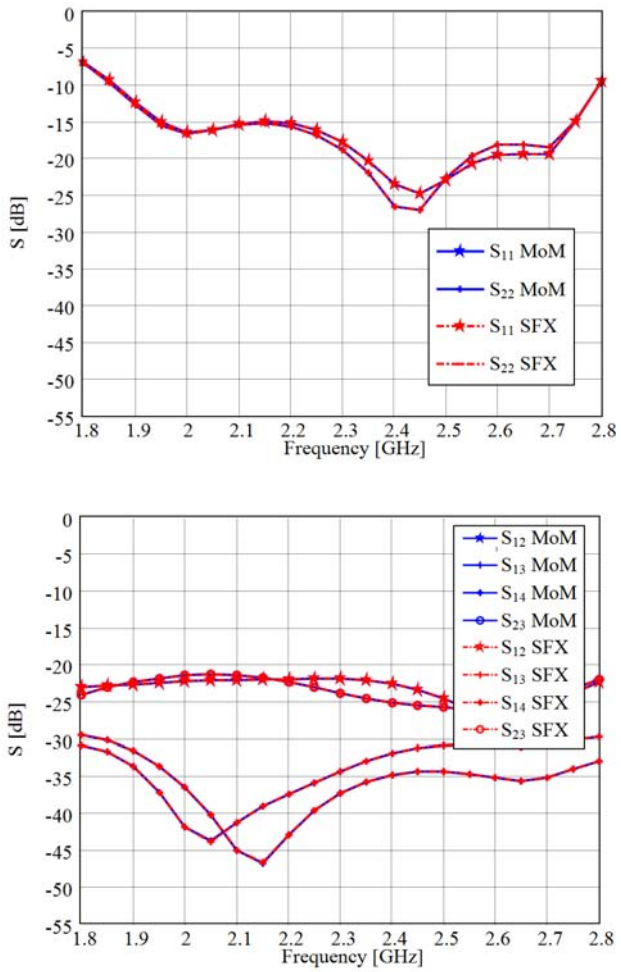

Fig. 6. Single column 4-patch array: Significant S parameters. Blue lines: standard MoM (reference); red lines: SFX.

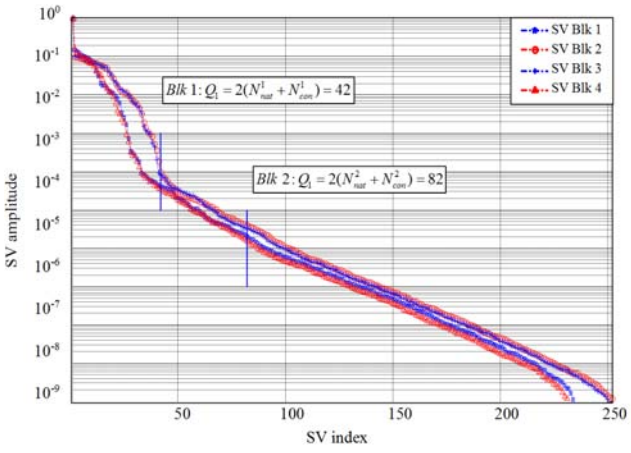

(a)

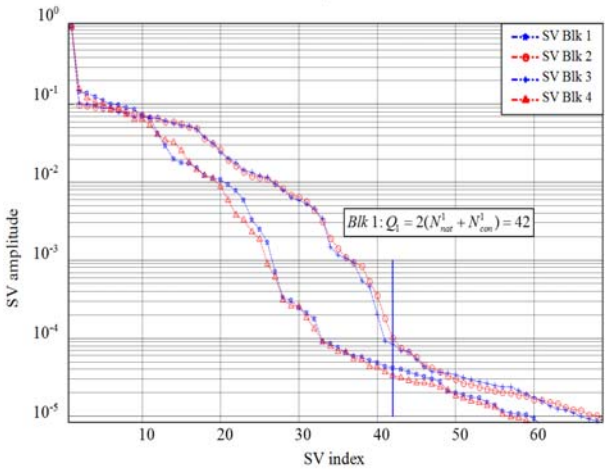

(b)

Fig. 7. Single column array (see Fig. 1): SV sequence. (a) Singular values sequence for the four s-blocks (superimposed); (b) Detailed view of the first part of the SV sequence. The vertical bars indicate the numbers Q.

Finally, Fig. 9 compares numerical and experimental results (reference MoM and SFX are undistinguishable); the agreement is very good (note that the slight shift in the resonance frequency happens below −20 dB in return loss).

As to numerical performances, using a $t \approx 10^{-5}$ threshold, the total dimension of the final linear equations system in the SFX basis has decreased to 658 unknowns (from 3010 unknowns in the RWG basis) and the solution time for this compressed system is of 4.9 seconds, which gives a cumulated solution time for all the 21 frequency steps of about 105 seconds. The necessary time for solving the 3010 unknowns linear equation system in the original RWG basis, for only one of the 21 frequency steps, is of 433.43 seconds. This means that the total solution time for all the 21 frequency steps in the original RWG basis is of 9102 seconds, 86 times the solution time in the SFX basis.

As the convergence results show, the $t = 10^{-5}$ value chosen for the SV threshold for this numerical simulation is very conservative. A higher compression of the final linear equation system, without significant changes in the accuracy of the final solution can be achieved also with $t = 10^{-3}$.

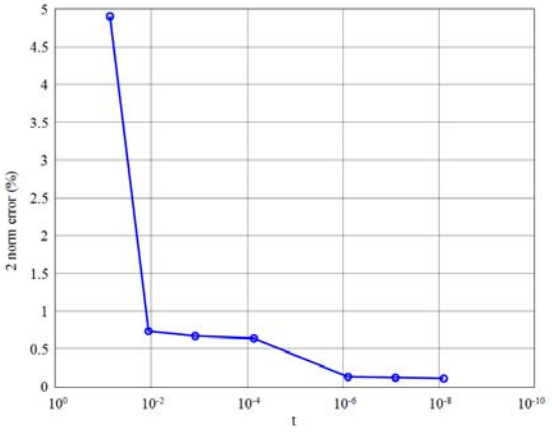

(a)

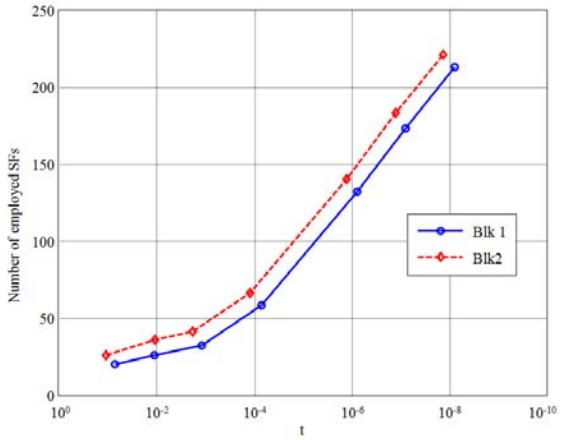

(b)

Fig. 8. Single column array (see Fig. 1). (a) Surface current error (18) with respect to SV threshold value t in (10); (b) Number of SFs corresponding to threshold values t; solid line: external blocks; dashed line: internal blocks.

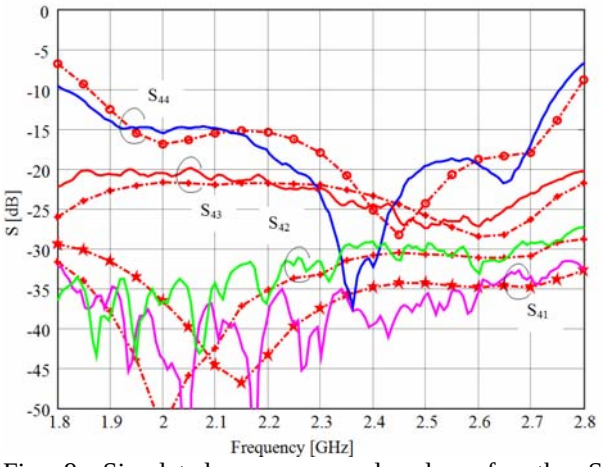

Fig. 9. Simulated vs. measured values for the S parameters of one column of the array considered in isolation; the curves without markers correspond to the measurements.

Analysis of the entire antenna

As alluded above, the only direct comparison between measured and simulated data is for the radiation pattern, yet including cross-pol. However, computed self- and mutual-impedances of the 32 radiating elements were employed in obtaining the radiation data; they were used to compute the excitation coefficients at all ports by solving the circuit problem with the S-matrix of the BFN splitters (data sheets and measured on prior breadboarding) and the S-matrix of the 32-element array.

The complete base station antenna in Fig. 1.a) was separated into the 16 blocks shown in Fig. 2 (exploded view of the mesh after block separation); each block contains two azimuthally neighboring radiating elements. Due to the symmetry of the structure and of the domain-decomposition, all blocks are identical to one of the two separately shown in Fig. 2, corresponding to internal or terminal location in the structure. Also in this case, we note that the block partitioning requires the cut of the continuous ground plane below the patches, i.e. the continuity of the current on it; this generates the need of connection functions and connection sources.

There are two natural responses for the block (4 natural SFs, arising from the separation into real and imaginary parts) originating from the port excitation of each one of the two radiating elements inside each block. In addition to natural and connection functions, a total of 56 coupling sources were used around each block.

The SV sequences for the different blocks are shown in Fig. 10, only for the two basic blocks shown in 2. The reported results refer to two threshold values: $T = 10^{-1}$ and $T = 10^{-2}$, the latter being very conservative. For $T = 10^{-1}$, the total number of SFX unknowns in the SFs basis was of 2354, and the solution time of about 204 seconds (about 3.4 minutes). With $T = 10^{-2}$ there were 4379 SFX unknowns, requiring 1358 seconds (about 22.6 minutes) to solve. The surface current distribution on the entire structure obtained for the higher accuracy SFX simulation is illustrated in Fig. 11.

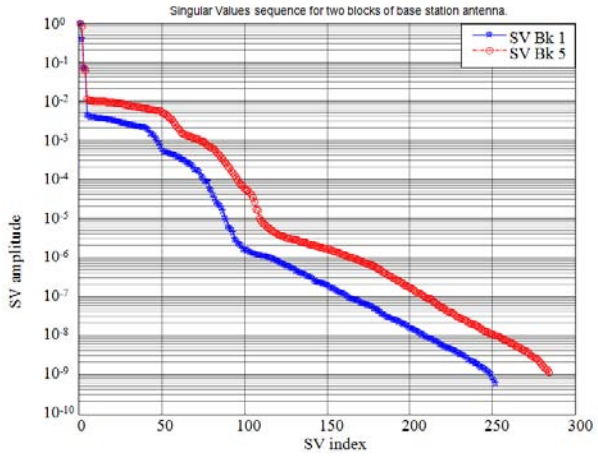

(a)

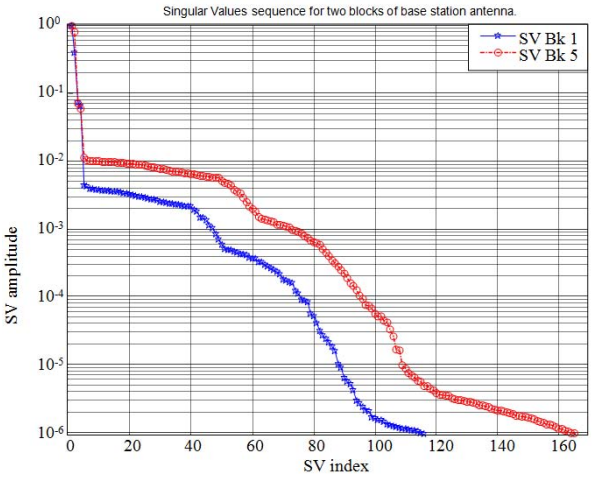

(b)

Fig. 10. (a) Singular values sequence for two blocks of conformal base station antenna; (b) detailed view of the first part of the SV sequence. For numbering see Fig. 2.

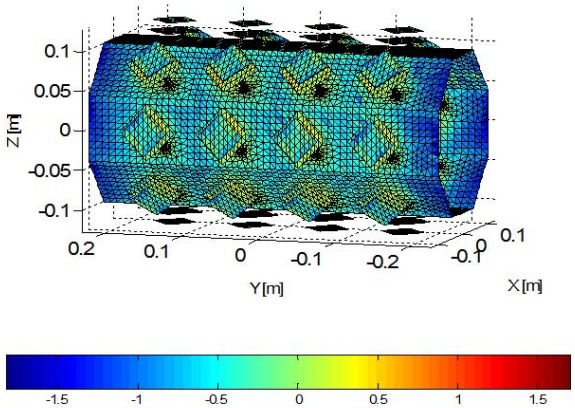

Fig. 11. Logarithmic plot for surface current on the base station antenna obtained by using the SFX technique.

The radiation patterns for the antenna were computed for the two sets of computed surface

currents and reported in Fig. 12 for the co-polar and cross-polar components. The results for the two solutions show negligible differences. The radiation patterns were measured for eight elevation cuts (vertical planes, Fig. 13), one cut for each facet, and in the horizontal plane (azimuth cut, Fig. 14). Despite the structural symmetry, some differences are observed, and most likely due to feed cables (especially beyond 140◦) and mast in addition to fabrication tolerances in the radiating elements and BFNs.

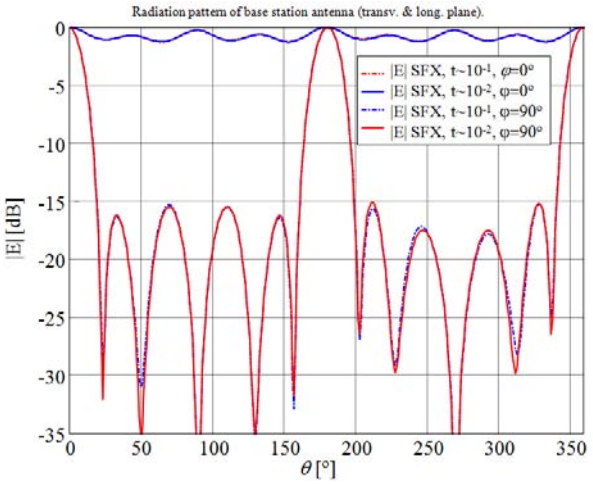

Fig. 12. SFX simulation results for base station antenna in Fig. 1; (a) radiation patterns in the two main planes for the base station antenna (solid line for T ≈ 10^{-2} threshold on SV sequence, dotted line for T ≈ 10^{-1} threshold); (b) Co- and cross-polar components (azimuthal cut) for the base station antenna (solid line for T ≈ 10^{-2}, dotted line for T ≈ 10^{-1}).

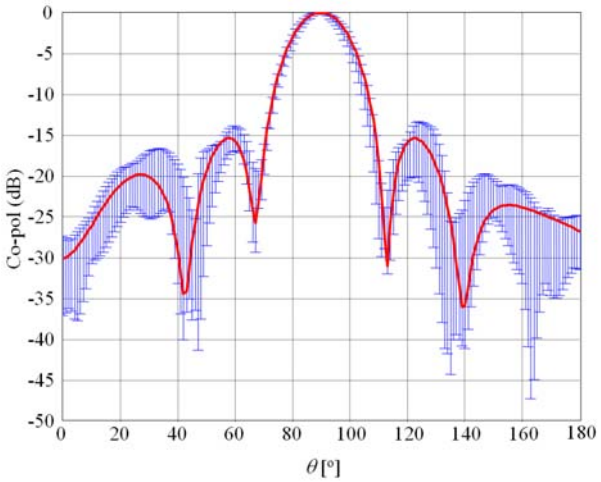

Fig. 13. Base station antenna: radiation pattern. The solid line shows computed results; the confidence bars display, for each angle, the min and max of the measured individual patterns for the 8 columns, in the plane orthogonal to each antenna facet.

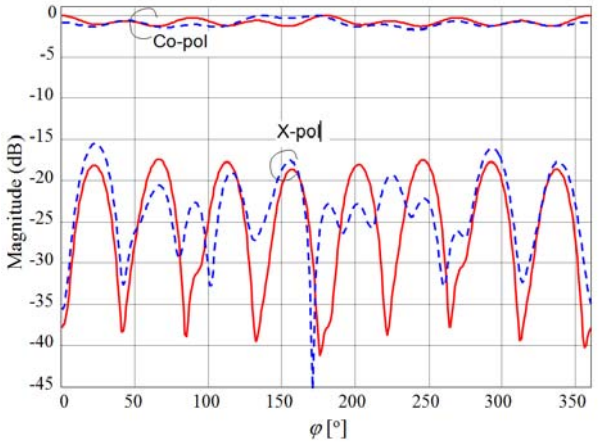

Fig. 14. Measured vs. simulated Co and Cross-polar components of the field for the entire array in azimuth cut.

IV.2 WBF

We will only consider simple examples so that we can use a simple fast 2D MoM algorithm due to the Toeplitz property of the resulting matrix. Nevertheless those easy examples contain all relevant difficulties to prove the method works, that is: concavity, multiple reflections, etc.. In all reported examples, we consider plane wave incidence along the directions indicated graphically in the relevant figures. The standard MoM (sub-wavelength) discretization uses triangular basis functions with $l = \lambda/10$ support; the number of associated basis functions will be denoted by N.

Scattering from flat strips were considered in [24]; here we discuss the case of scattering from a curved, concave strip; it is an arc of circle of angular aperture λ/2 and arc length L sketched in the inset of Fig. 15; the incidence is from the direction bisecting the opening angle ($\phi_{inc} = \pi/4$) in the concave part. Two cases were considered: L = 360λ, with N = 3600 and NWBF = 273, with support of about 6λ; and L = 1440λ, with N = 14400 but with the same NWBF as in the previous case, i.e. with aggregate function of about 24λ.

The error on the current, defined as in (18) (with SFX substituted for WBF), was 3.5% for the L = 360λ case, and 1.8% for the larger, L = 1440λ case. It is interesting to note that the number of necessary WBF terms is essentially independent of the frequency. This observation seems confirmed by [30]. The comparison for the radiated (far) field is shown in Fig. 15 for the case of L = 1440λ; panel (a) shows the overall pattern, and the following panels (b-h) report enlargement of various zones, to allow for a closer comparison. The figure allows to appreciate the accuracy of the WBF approach; the deviation from standard MoM is negligible almost everywhere, with small deviations in a low-amplitude region (panel d; well below -30dB).

V. CONCLUSION

We have discussed integral-equation methods that employ basis functions constructed by grouping standard ”elemental” basis functions (e.g. RWG); these basis functions are termed ”aggregate” throughout. The initial general setting includes both one-to-one basis change, that leave the number of unknowns unchanged, and compressive mappings, that reduce the overall number of necessary unknowns. In the former case, the reasons behind the basis change are typically centered around the spectral properties of the ensuing MoM matrix, like in the loop-tree decomposition used at low frequencies.

The discussion then has been focused on compressive aggregate-function methods. General considerations have been offered, and the specific examples of SFX and WBF methods employed to substantiate the general discussion. The SFX method belongs to the larger class of domain-decomposition methods, while WBF is based on high-frequency local solutions of Maxwell equations.

Compressive methods appear to be a mature technology in Computational EM; they can provide a simple ”boost” solution that re-uses existing MoM codes, but they can also be used to produce sophisticated tools. In particular, their combination with fast methods appears very promising, due to the complementary natures of the two approaches.

ACKNOWLEDGMENTS

The authors would like to acknowledge the cooperation with Prof. M. Orefice and Ing. G.L. Dassano for the design and measurement of the base station antenna employed as an application example in this paper.

This work has been partially developed in the Sixth Framework Program of the European Community within the Antenna Center of Excellence (ACE2). This work has been supported in part by the Spanish Ministerio de Educacion y Ciencia under the project TEC2004-04866-C04.

REFERENCES

[1] T. F. Eibert,“Iterative-solver convergence for loop star and loop-tree decomposition in method of moments solutions of the electricfield integral equation”, *IEEE Antennas Propagat. Mag.*, vol. 46, no. 3, pp. 80, pp. 2509−2521, 2004.

[2] S. Ooms and D. DeZutter, “A new iterative diacoptics based multilevel moments method for planar circuits”, *IEEE Trans. Microw. Theory Tech.*, vol. MTT-46, no. 3, pp. 280, pp. 2509−2521291, 1998.

[3] J. Heinstad, “New approximation technique for current distribution in microstrip array antennas”, *Electron. Lett*., vol. 29, no. 21, pp. 1809−1810, 1993.

[4] E. Suter and J. Mosig, “A subdomain multilevel approach for the MoM analysis of large planar antennas”, *Microw. Opt. Technol. Lett.*, vol. 26, no. 4, pp. 270−277, 2000.

[5] V. V. S. Prakash and R. Mittra, “Characteristic basis function method: a new technique for efficient solution of method of moments matrix equation”, *Microw. Opt. Technol. Lett*., pp. 95−100, 2003.

[6] L. Matekovits, G. Vecchi, G. Dassano, and M. Orefice, “Synthetic Function Analysis of Large Printed Structures: the Solution Space Sampling Approach”, *Digest of 2001 IEEE AP-S Soc. Int’l*

Symp., pp. 568−571, 8−13, July 2001, Boston, Massachusetts, USA.

[7] L. Matekovits, V. A. Laza, and G. Vecchi, "Analysis of Large Complex Structures with the Synthetic Functions Approach", *IEEE Trans. Antennas and Propagat*., vol. 55, no. 9, pp. 2509−2521, 2007.

[8] K. F. Sabet, J. C. Cheng, and L. P. B. Katehi, "Efficient wavelet-based modelling of printed circuit antenna arrays", *IEE Proc. Microwave Antennas Propagat.*, vol. 146, no. 4, pp. 298−304, 1999.

[9] R. Loison, R. Gillard, J. Citerne, G. Piton and H. Legay, "Optimised 2D multi-resolution method of moment for printed antenna array modelling", *IEE Proc. Microwave Antennas Propagat.*, vol. 148, no. 1, pp. 1−8, 2001.

[10] P. Pirinoli, G. Vecchi, and L. Matekovits, "Multiresolution analysis of printed antennas and circuits: a dual−isoscalar approach", *IEEE Trans. Antennas Propagat.*, vol. 49, no. 6, pp. 858−874, 2001.

[11] G. Schneider, G. Oberschmidt, and A. F. Jacob, "Efficient Implementation of a Wavelet Based Galerkin Scheme", *IEEE Trans. Antennas Propagat.*, vol. 52, no. 9, pp. 2298−2304, 2004.

[12] F. Vipiana, P. Pirinoli, and G.Vecchi, "A Multiresolution Method of Moments for Triangular Meshes", *IEEE Trans. Antennas Propagat.*, vol. 53, no. 7, pp. 2247−2258, 2005.

[13] Z. Baharav, Y. Leviatan "Analysis Of Scattering By Surfaces Using A Wavelet- Transformed Triangular-Patch Model", *Microwave Opt. Tech. Lett.*, vol. 21, no. 5, pp. 359−365, 1999.

[14] W. C. Bandlow, G. Schneider, and A. F. Jacob, "Vector-valued wavelets with triangular support for method of moments applications", *IEEE Trans. Antennas Propagat.*, vol. 53, no. 10, pp. 3340−3346, 2005.

[15] F. Vipiana, G. Vecchi, and P. Pirinoli, "A Multi-Resolution system of Rao-Wilton-Glisson functions", *IEEE Trans. Antennas Propagat*., vol. 55, no. 3, pp. 924−930, 2007.

[16] F. P. Andriulli, F.Vipiana, and G.Vecchi, "Hierarchical bases for non-hierarchic 3D triangular meshes", *IEEE Trans. Antennas Propagat.*, vol. 56, no. 8, pp. 2288−2297, 2008.

[17] F. Vipiana, P. Pirinoli, and G.Vecchi, "Spectral properties of the EFIE-MoM matrix for dense meshes with different types of bases", *IEEE Trans. Antennas Propagat*., vol. 55, no. 11, pp. 3229−3238, 2007.

[18] C. Craeye, "A Fast Impedance and Pattern Computation Scheme for Finite Antenna Arrays", *IEEE Trans. Antennas Propagat.*, vol. 54, no. 10, pp. 3030−3034, 2006.

[19] P. De Vita, A. Freni, L.Matekovits, P. Pirinoli, and G.Vecchi, "A combined AIM-SFX approach for complex arrays", *Digest of 2007 IEEE APS Soc. Int'l Symp.*, pp. 3452−3455, Honolulu, Hawaii, USA, 10−15 June 2007.

[20] V. A. Laza, L. Matekovits, and G. Vecchi, "Synthetic Function Expansion with multi-grid approach", *Proceedings of The First European Conference on Antennas and Propagation* (*EuCAP 2006*), ESA SP-626 CD Proceedings, pp. 386.1, Nice, France, 6−10 November 2006.

[21] F. C´atedra, E. Garca, C. Delgado, F. S. de Adana, and R. Mittra, "Development of an efficient rigorous technique based on the combination of CBFM and MLFMA to solve very large electromagnetic problems", *Proc. Int'l Conf. Electromagnetics in Advanced Applications*, Torino, Italy, Sep. 2007.

[22] R. Maaskant, R. Mittra, and A. Tijhuis, "Fast Solution of Multi-Scale Antenna Problems for the Square Kilometre Array (SKA) Radio Telescope using the Characteristic Basis Function Method (CBFM) ", *Applied Computational Electromagnetics Society Journal*, vol. 24, no. 2, 2009

[23] O. M. Bucci, and G. Franceschetti, "On the degrees of freedom of scattered fields", IEEE Trans. Antennas and Propagat., vol. 37, no. 7, pp. 918−926, 1989.

[24] F. Vico, G. Vecchi, M. Ferrando, "A New Sparsification And Compression Technique For High Frequency Mom By Means Of Wavefront Basis Functions", *Proceedings of The First European Conference on Antennas and Propagation EuCAP, 2007*.

[25] K. R. Aberegg and A. F. Peterson, "Application of the Integral Equation-Asymptotic Phase Method to two-dimensional scattering", *IEEE Trans. Antennas Propagat.*, vol. 43, no. 5, pp. 534−537, 1995.

[26] D. Kwon, R. J. Burkholder, and P. H. Pathak, "Efficient Method of Moments Formulation for Large PEC Scattering Problems Using Asymptotic Phasefront Extraction (APE)", *IEEE Trans. Antennas Propagat*., vol. 49, no. 4, pp. 583−591, 2001.

[27] S. N. Chandler-Wilder, S. Langdon, "A Galerking Boundary Element Method for High Frequency Scattering by Convex Polygons", *SIAM J. Numer. Anal*., vol. 45, no. 2, pp. 610−640, 2007.

[28] K. Tap, R. J. Burkholder, P. H. Pathak, and M. Albani, "Methods for Efficiently Computig the MoM Impedance Matrix for APEx Type Basis Functions", *IEEE AP-S Soc. Int'l Symp.*, pp. 4119−4122, Albuquerque, *2006*.

[29] R. J. Burkholder, and T. Lee, "Adaptive Sampling for Fast Physical Optics Numerical Integration", IEEE Trans. Antennas and Propagat., vol. 53, no. 5, pp. 1843−1845, 2005.

[30] C. P. Davis and W. C. Chew, "Frequency-Independent Scattering from a Flat Strip with TE_z-Polarize Fields", *IEEE Trans. Antennas Propagat.*, vol. 56, no. 4, pp. 1008−1016, 2008.

[31] S. Raffaelli, M. Johansson, and B. Johannisson, "Cylindrical Array Antenna Demonstrator for WCDMA Applications", *Proc. of ICEAA03*, Turin, Italy, 8−12 Sept. 2003.

[32] G. Vecchi, P. Nepa, G. Manara, A. Serra, M. Orefice, V. A. Laza, L. Matekovits, G. L. Dassano, and V. Kysrytsya, "Wideband Stacked-Patch Designs for Base Station Antenna", *Wireless Reconfigurable Terminals and Platforms* (*WiRTeP*), pp. 241−245, Rome, Italy, 10−12 April 2006.

[33] G. Dassano, V. A. Laza, L. Matekovits, M. Orefice, and G. Vecchi, "Numerical and Experimental Characterization of a Wide- Band Conformal Base Station Antenna", *Digest of 2006 IEEE AP-S Soc. Int'l Symp*., pp.3735−3738, Albuquerque, New Mexico, 9−14 July 2006.

Ladislau Matekovits was born in Arad (Romania), on November 19, 1967. He received the degree in Electronic Engineering from Institutul Politehnic din Bucureşti, Bucureşti, Romania and the Ph.D. (Dottorato di Ricerca) in Electronic Engineering from Politecnico di Torino, Turin, Italy in 1992 and 1995 respectively. Since 1995 he has been with the Electronics Department of the Politecnico di Torino, first with a post-doctoral fellowship, then as a Research Assistant. He joined the same Department as Assistant Professor in 2001 and was appointed as Senior Assistant Professor in 2005. In late 2005 Ladislau Matekovits was Visiting Scientist at the Antennas and Scattering Department of the FGAN-FHR, Wachtberg, Germany. His main research interest is in the numerical analysis of printed antennas and in particular in the development of new, numerically efficient full-wave techniques to analyze large arrays, in metamaterials and in optimization techniques. Dr. Matekovits is recipient of many awards in international conferences, and is member of various conferences program committees. He was Assistant Chairman and Publication Chairman of the European Microwave Week 2002 (Milan, Italy). He serves as a reviewer for the various Journals in his fields of interest.

Giuseppe Vecchi received the Laurea and Ph.D. (Dottorato di Ricerca) degrees in electronic engineering from the Politecnico di Torino, Torino, Italy, in 1985 and 1989, respectively, with doctoral research carried out partly at Polytechnic University (Farmingdale, NY). He was a Visiting Scientist at the Polytechnic University from August 1989 to February 1990. In 1990, he joined the Department of Electronics, Politecnico di Torino, as an Assistant Professor (Ricercatore) where, from 1992 to 2000, he was an Associate Professor and, since 2000, he has been a Professor. He was a Visiting Scientist at the University of Helsinki, Finland, in 1992, and has been an Adjunct Faculty in the Department of Electrical and Computer Engineering, University of Illinois at Chicago, since 1997. His current research activities concern analytical and numerical techniques for analysis, design and diagnostics of antennas and devices, RF plasma heating, electromagnetic compatibility, and imaging.

Felipe Vico was born in Valencia, Spain, in 1981. He received the M.S in 2004 in telecommunication from the Polytechnic University of Valencia. From 2004 to 2005 he was with the Institute of Telecommunications and Multimedia Applications (iTEAM) as a Research Assistant. From 2005 to 2006 he was awarded with a Research Fellowship by the Spanish Ministry of Culture. Since 2007 he has been an Assistant Professor in the Communications Engineering Department, Polytechnic University of Valencia, where he is currently working toward the Ph.D degree. His research interests include numerical methods applied to scattering and radiation problems, asymptotic techniques, hybridization of high frequency and numerically rigorous methods and fast computational techniques applied to electromagnetics.